Faraday Discussions

Cite this: DOI: 10.1039/d4fd00164h

ROYAL SOCIETY OF CHEMISTRY

PAPER

View Article Online
View Journal

Impacts of Arctic oil field NO_x emissions on downwind bromine chemistry: insights from 5 years of MAX-DOAS observations

Peter K. Peterson, *[a] Kerri A. Pratt, [b] Paul B. Shepson[cd] and William R. Simpson [e]

Received 7th October 2024, Accepted 25th November 2024
DOI: 10.1039/d4fd00164h

Oil and gas production is a substantial source of nitrogen oxides to the atmosphere, with significant impacts particularly in remote regions without other large local NO_x sources. In the Arctic, these emissions impact regional halogen and HO_x chemistry, altering the oxidation of atmospheric pollutants. In this work we utilize Multiple Axis Differential Optical Absorption Spectroscopy (MAX-DOAS) NO_2 and BrO measurements at Utqiaġvik, Alaska, from 2012 to 2016. During the spring months when atmospheric bromine chemistry is most prevalent, we find 8% of observations are impacted by observed NO_2 differential slant column densities (dSCDs) over 5×10^{15} molecules per cm^2, which we classify as polluted. Of this fraction, approximately half can be attributed to sources outside the immediate vicinity of Utqiaġvik. During these polluted times, observed BrO lower tropospheric column densities (LT-VCDs) are 60% lower on average than those retrieved during non-polluted times. During times when the local wind direction corresponds with a large collection of oil and gas extraction facilities approximately 300 km southeast of Utqiaġvik, observed BrO LT-VCDs were 30% lower than clean air times. These observations show that current oil and gas operations in the Arctic are impacting the natural atmospheric photochemical processes.

1 Introduction

Snowpack-driven atmospheric bromine chemistry is a prominent natural feature of the springtime Arctic.[1] This chemistry is responsible for the episodic depletion of boundary layer ozone to near-zero levels, commonly referred to as ozone depletion events or ODEs,[2] and altered oxidation of atmospheric pollutants like

[a]Department of Chemistry, Whittier College, Whittier, USA. E-mail: ppeterso@whittier.edu; Tel: +1 562 907 5149
[b]Department of Chemistry, University of Michigan, Ann Arbor, USA
[c]Department of Chemistry, Purdue University, West Lafayette, USA
[d]School of Marine and Atmospheric Science, Stony Brook University, Stony Brook, USA
[e]Department of Chemistry and Biochemistry, Geophysical Institute, University of Alaska Fairbanks, Fairbanks, USA

mercury.[3] Molecular halogens, including Br_2, are photochemically produced in the snowpack with the return of sunlight in the polar spring.[4,5] The photolysis of Br_2 leads to the production of bromine atoms which then rapidly react with ozone to form BrO.[6] While BrO will photolyze to regenerate ozone and bromine atoms, it can also react with itself (R1–R3), or other oxides, leading to the depletion of ozone.[6]

$$Br_2 + h\nu \rightarrow 2Br \quad (R1)$$

$$Br + O_3 \rightarrow BrO + O_2 \quad (R2)$$

$$BrO + BrO \rightarrow Br_2 + O_2 \quad (R3)$$

Alternatively, BrO can also react to form HOBr which, under acidic conditions, can then react with bromide on the snowpack[4] or aerosol particles contributing to the further release of Br_2[7] and enabling the transport of reactive bromine beyond its source.[8,9]

$$BrO + HO_2 \rightarrow HOBr + O_2 \quad (R4)$$

$$HOBr + Br^-_{(aq)} + H^+_{(aq)} \rightarrow Br_2 + H_2O \quad (R5)$$

NO_x ($NO + NO_2$) can also play an important role in this chemistry.[10] While it reacts directly with BrO, decreasing the rates of R3 and R4 to slow gas phase bromine chemistry, the product, $BrONO_2$ can also contribute to recycling in the same manner that HOBr does in R5.[6,7,11,12]

$$BrO + NO_2 \rightarrow BrONO_2 \quad (R6)$$

$$BrONO_2 + Br^-_{(aq)} \rightarrow Br_2 + {NO_3}^-_{(aq)} \quad (R7)$$

$$BrONO_2 + H_2O \rightarrow HOBr + HNO_3 \quad (R8)$$

The relative importance of these competing effects and the overall impact on atmospheric bromine chemistry are highly dependent on the concentrations of NO_x.[10] NO_x mole fractions are typically quite low in the remote Arctic, below 100 pmol mol^{-1}, with the primary source being production in the snowpack.[13,14] However, in populated areas or regions with ongoing resource extraction, these mole fractions can be much higher due to local NO_x emissions. Given ongoing warming and summer sea ice extent declines in the Arctic,[15] it is expected that shipping activity and resource extraction, and their associated NO_x emissions, will increase.[16] Thus, understanding the interplay between anthropogenic NO_x emissions and naturally occurring halogen chemistry is an increasingly key need.

Multi-year ground-based observations have provided an important tool to study this bromine chemistry across the Arctic in Eureka, Canada,[17] on sea ice tethered buoy networks,[18–21] and at Utqiaġvik,[19–21] USA. Utqiaġvik is the largest city on the North Slope of Alaska, and thus has a substantial amount of local anthropogenic emissions that impact concentrations of key atmospheric constituents. Transported emissions from other sources have also been identified as a key contributor to local air pollution, including for NO_x,[22–24] methane,[23,25] and

aerosol particles.[26–28] Prudhoe Bay, one of several oil fields on the North Slope of Alaska, is approximately 300 km SE of Utqiaġvik and one of the largest oil producing regions in North America, and has a large number of oil and gas extraction facilities.

In this work we utilize measurements of BrO and NO_2 collected over a five year period in conjunction with Stochastic Time-Inverted Lagrangian Transport (STILT) modeling[29] to determine the frequency of impacts to Utqiaġvik from Prudhoe Bay oil field emissions, and assess the impacts on atmospheric bromine chemistry observed in the polar spring.

2 Methods

2.1 MAX-DOAS

Multiple Axis Differential Optical Absorption Spectroscopy (MAX-DOAS)[30] was utilized to measure BrO and NO_2 from the top of the Barrow Arctic Research Consortium (BARC) building, located 6 km NE of Utqiaġvik (71.325 N°, 156.668° W) from March of 2012 through June of 2018. Details about the instrument and retrieval methods are described in detail in prior work.[31,32] Briefly, differential slant column densities (dSCDs) for BrO, O_4, and NO_2 were measured at nominal −2, −1, 0, 1, 2, 3, 5, 10, and 20° elevation angles. A zenith spectrum collected with each scan was used as reference spectrum. The retrieval of BrO profiles from dSCD measurements is a two step process. First, the measured O_4 dSCDs are used to retrieve a vertical profile of aerosol particle extinction,[33] which can also be integrated to provide aerosol optical thickness. This retrieved profile is then used as an additional input to constrain light scattering in the next step of the retrieval, where BrO dSCDs are used to retrieve vertical profiles of BrO using optimal estimation.[33–36]

Because the retrieved BrO profiles generally have only 2–3 degrees of freedom, rather than utilizing the retrieved profiles, we reduced them to two reported quantities,[37] the average mole fraction in the lowest 200 m, the lower tropospheric vertical column density (LT-VCD) which represented the total column of BrO between 0 and 2 km. These two quantities are also used to calculate the f_{200}, the fraction of BrO in the lowest 200 m of the atmosphere.[31] While measurements exist over a wider time frame, given our intent to examine impacts on bromine chemistry active in the polar spring, we only utilize data collected from polar sunrise to June 1st for all years, a time span which encompasses all snow melt onset dates observed at Utqiaġvik during the study period.[20] BrO LT-VCDs were below detection limits outside of this period.

2.2 Identification of oil and gas field influenced periods

Stochastic Time-Inverted Lagrangian Transport (STILT) modeling[29] was utilized to determine the footprint of sensitivity to upwind emissions of Utqiaġvik over the course of the study (Fig. 1). These footprint calculations rely on 1° meteorological fields derived from National Centers for Environmental Prediction Global Data Assimilation System (GDAS). To determine the degree to which a given observation was influenced by emissions from oil and gas extraction activities on the North Slope of Alaska, we summed the calculated footprint over the Prudhoe Bay and adjacent oil fields, indicated by the black box in Fig. 1, and designated times

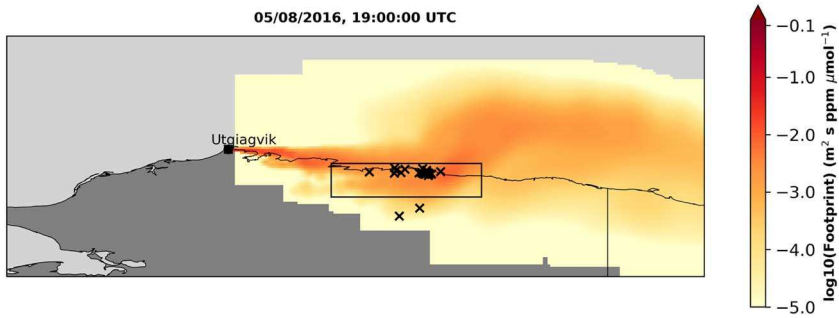

Fig. 1 Example STILT footprint is shown overlain on map of northern Alaska. The black box encompasses oil fields on the North Slope of Alaska, including Prudhoe Bay. Individual emission sources that report to the US Environmental Protection Agency Greenhouse Gas Reporting Program are marked with a black ×. These data are plotted on a log scale to enhance contrast.

when the value of this summed footprint exceeded 0.1 m^2 s ppm μmol^{-1} (units of ppm enhancement per unit of flux) as Prudhoe Bay influenced.

2.3 CIMS

During the spring 2016 Photochemical Halogen and Ozone Experiment: Mass Exchange in the Lower Troposphere (PHOXMELT) campaign, HO_2NO_2 and HNO_3 were measured at 1 m above the snowpack at a tundra site (71.275°N, 156.641°W), located five km south of the BARC building across flat tundra.[24] The iodide–water cluster chemical ionization mass spectrometry measurements[38] were conducted and calibrations performed as described by McNamara *et al.*[24] Hourly average HO_2NO_2 mole fractions and HNO_3 mole fractions are reported here,[39] with uncertainties of 30% + 4 pmol mol^{-1} (1 h LOD). HO_2NO_2 data were available from Mar 4th to May 20th 2016. HNO_3 was only quantified from April 8th to May 20th due to high background signal earlier in the study.

2.4 Other datasets

Ozone data used in this work were provided by the National Oceanic and Atmospheric Administration (NOAA) Earth Systems Research Laboratory/Global Monitoring Division (ESRL/GMD).[40] Wind speed and direction measurements were also provided by NOAA.

3 Results and discussion

3.1 Air mass categorization

Air masses were categorized using observed NO_2 dSCDs, local wind direction measurements, and STILT footprints. Observations were categorized as being influenced by recent anthropogenic pollution if the observed 2° NO_2 dSCD was in excess of 5×10^{15} molecules per cm^2.[21] Wind direction and NO_2 measurements were utilized to categorize air masses into three categories, as illustrated in Fig. 2. Clean air (275–55° east of north) refers to the traditional clean air sector that is determined to be free of local emission influence.[25] Non-local refers to

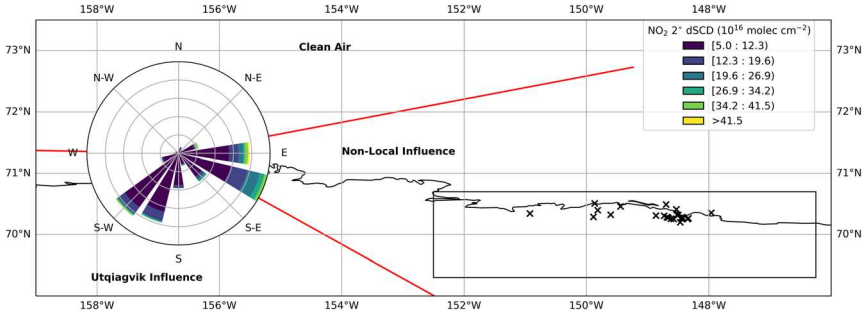

Fig. 2 Plot of NO_2 dSCDs plotted as a function of wind direction centered on the BARC building. This plot shows the wind directions associated with NO_2 observations in excess of 5×10^{15} molecules per cm^2. The North Slope of Alaska oil fields are outlined with a rectangle and individual emission sources that report to the US Environmental Protection Agency Greenhouse Gas Reporting Program are marked with a black $\times$.

measurements outside the clean air sector that are not in the direction of Utqiaġvik (55–145° east of north), but exhibit enhancements in observed NO_2. Of these non-local air masses, those determined to be impacted by oil and gas extraction activities using STILT footprints were then placed in a separate category labeled Prudhoe Bay. Measurements where the wind was blowing from the city of Utqiaġvik (145–275° east of north) are labeled as Utqiaġvik.

Of the resulting categorized BrO data set, 27% of observations were clean air, 36% were not attributable to Utqiaġvik or Prudhoe Bay, 18% were influenced by Prudhoe Bay, and 19% were impacted by local emissions from Utqiaġvik. 8% of BrO observations were determined to be influenced by recent anthropogenic pollution using NO_2 dSCD measurements. Of these observations, 42% were impacted by Prudhoe Bay and 35% were impacted by Utqiaġvik, illustrating that these areas are responsible for the majority (77%) of NO_x enhancements observed at Utqiaġvik.

3.2 Effectiveness of STILT as a quantitative metric

Prior efforts to identify impacts of oil and gas extraction activities on Utqiaġvik have relied on wind speed and direction[22,23] and/or HYSPLIT backward air mass trajectory modeling,[24,27,28] which result in a binary classification of these impacts. Here we utilize STILT footprints to quantify the degree to which an observed air mass is impacted by long range transport from Prudhoe Bay. Given that NO_2 has a relatively short lifetime, and is generally indicative of fresh anthropogenic air pollution, the magnitude of NO_2 enhancements will be highly dependent on the time for an air mass to be transported from Prudhoe Bay to Utqiaġvik. Assuming a distance of 300 km and utilizing wind speed measurements to estimate a transport time suggests a range of between six and forty hours for air masses in the Prudhoe category over the course of this study. Thus, utilizing measurements of NO_x reservoir species (*i.e.* NO_z) like those utilized in prior work by Jaffe *et al.*[23] is a preferable approach to evaluating this method to identify impacted times. Since NO_z measurements were not available over the whole study period, we utilized the NO_z components HO_2NO_2 and HNO_3 made during the 2016 PHOXMELT

campaign to examine the impacts of these upwind emissions. Excluding observations from the Utqiaġvik sector, both species mole fractions exhibit positive correlations with the summed STILT footprint (Fig. 3), with HNO_3 having a stronger correlation ($R = 0.69$) than HO_2NO_2 ($R = 0.43$) during March–May of 2016. This finding potentially reflects the shorter atmospheric lifetime of HO_2NO_2, which is on the order of minutes[41] compared to HNO_3 which can have a lifetime on the order of days,[42] although this lifetime is highly dependent on mixing height, with shallower boundary layers leading to increased dry deposition rates.[43] These findings suggest this method is able to generally quantify the degree of influence from oil and gas fields on the North Slope on observations at Utqiaġvik even without accounting for temporal and spatial variations in NO_x emissions in these extraction areas.

Utilization of STILT shows that measurements at Utqiaġvik are impacted by the North Slope oil fields 18% of the time which is much higher than indicated by local NO_2 measurements, which only indicated impacts from these regions 3% of the time. When examining the three initial categories selected based solely on wind sector (Fig. 2), each of the initial sector assignments is impacted to varying degrees by oil and gas extraction emissions. 23% of the observations with winds corresponding to the non-local sector are impacted by oil and gas extraction emissions, 11% of the clean air sector observations are impacted, and 16% of the Utqiaġvik observations are also impacted by these emissions.

3.3 Impacts on BrO

Fig. 4 shows that BrO LT-VCDs generally decrease with increasing influence of Prudhoe Bay emissions. Any observed enhancements of NO_2 are also generally associated with near-zero BrO LT-VCDs, suggesting a conversion of BrO_x to $BrONO_2$ or $BrNO_2$. This finding is consistent with prior airborne observations over

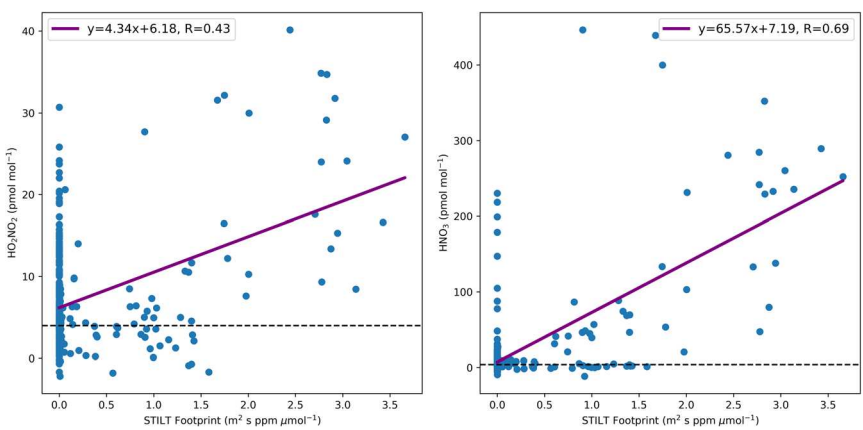

Fig. 3 Hourly HO_2NO_2 (left) and HNO_3 (right) mole fractions plotted as a function of the amount of time the observed air mass spent over oil fields on the North Slope of Alaska as determined by summed STILT footprint for all measurements outside the Utqiaġvik sector. The line of best fit is shown with a purple line and linear correlation coefficients for both species are indicated along with the line of best fit. The LOD (4 pmol mol^{-1}) for both measurements is indicated with a black line.

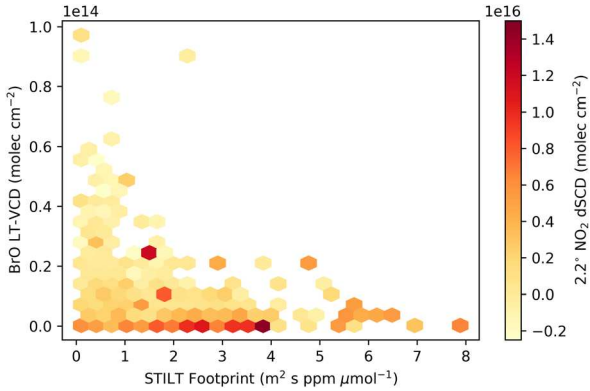

Fig. 4 Hexagonally binned scatter plot of BrO LT-VCDs plotted as a function of the amount of time the observed air mass spent over Prudhoe Bay as determined by summed STILT footprint for all observations designated as impacted by Prudhoe Bay. The color scale denotes the average NO_2 observation in each bin.

Prudhoe Bay by Custard *et al.*[10] that showed an anti-correlation between NO_2 and BrO. However, most observations, even those with a large degree of influence from North Slope oil and gas field emissions, are marked by low NO_2 (dSCD < 5×10^{15} molecules per cm^2), reflecting the short lifetime of NO_x and its conversion to other species like HO_2NO_2 and HNO_3 (Fig. 3).

The distribution of BrO observations across categories is shown in Fig. 5. A one way analysis of variance indicates all differences between categories are statistically significant with the exception of aerosol optical thickness. The clean air sector exhibited both the highest median BrO LT-VCD (median = 1.6×10^{13} molecules per cm^2) and lowest median ozone (13 nmol mol^{-1}). The fraction of

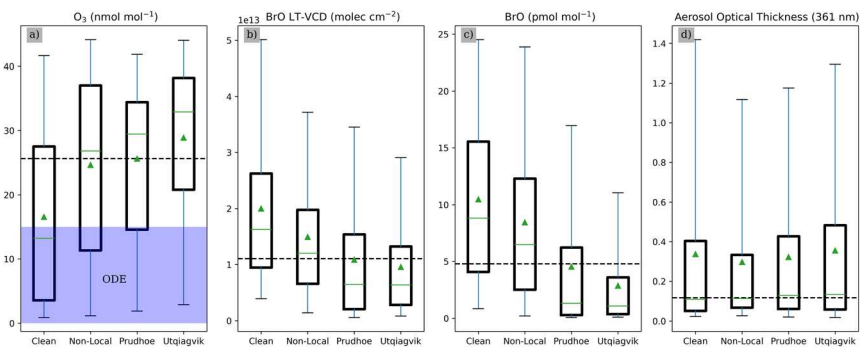

Fig. 5 Box and whisker plots of ozone (a), BrO LT-VCD (b), BrO mole fractions in the lowest 200 m (c), and aerosol optical thickness (d) binned by air mass categorization. The whiskers extend from the 5th to 95th percentile and the black box bins the 25th to 50th percentile. Means and medians for each bin are indicated with green triangles and lines respectively. On panel (a), blue shading indicates ozone values less than 15 nmol mol^{-1} indicating an ODE.[18] Aerosol optical thickness retrievals from MAX-DOAS observations do not differentiate between aerosols and clouds, leading to higher AOTs. All plots show the median for the overall data set with a dashed line.

ozone observations below 15 nmol mol^{-1}, was also highest in this sector, consistent with prior studies of ODEs at Utqiaġvik.[44] BrO LT-VCDs were generally lower for observations not attributed to the clean air sector, with the lowest median BrO LT-VCDs being observed when observations were impacted by Utqiaġvik or Prudhoe Bay (median = 6.4×10^{12} molecules per cm^2). Median ozone mole fractions were higher and few ozone observations at levels consistent with ODEs were observed in these impacted categories. These increased ozone mole fractions also potentially reflect the production of ozone due to the oxidation of volatile organic compounds co-emitted with NO_x in these regions.[45,46] While BrO observations are highest in the clean air sector, BrO LT-VCDs in the top quartile (>2×10^{13} molecules per cm^2) of the five year period and instances of ozone depletion events were observed for all four categories shown in Fig. 5. The relationship between BrO and ozone observed in this study across categories are consistent with prior work highlighting the role of bromine in ODEs.[2,47]

The finding of bromine chemistry being most active in the clean air sector potentially reflects the large role snow covered sea ice regions play in halogen activation chemistry,[19,48] and air masses arriving from this sector having spent the majority of their time in snow-covered sea ice regions. Prior work showed that air masses observed at Utqiaġvik that spend less than six hours of time in sea ice regions have an average BrO LT-VCD of 5.5×10^{12} molecules per cm^2, but also showed that the effects of time spent in sea ice regions on BrO are limited after ~36 hours.[19] While observations in other sectors may not have the same degree of sea ice influence, the coastal snowpack is still an effective enabler of bromine chemistry[4,5] and this chemistry has been observed over snowpacks 200 km south of Utqiaġvik.[49] Additionally, given the prevailing regional sea ice conditions in the polar spring, the majority of observations are of air masses that have spent more than six hours over sea ice regions regardless of sector. Thus, variations in the degree of sea ice influence, while a factor, likely cannot explain the entirety of the differences in observed BrO columns between sectors.

Oil fields on the North Slope of Alaska and the city of Utqiaġvik are both characterized by anthropogenic NO_x emissions that can consume BrO_x through direct reaction with NO_2 to form $BrONO_2$ and $BrNO_2$. These reactions serve as termination steps for BrO_x, shortening the bromine radical chain length, in turn slowing the rate of ozone depletion.[50] The observation of decreased BrO LT-VCDs in both of these sectors as compared to other sectors (Fig. 5) is consistent with this hypothesis. During the 2016 PHOXMELT campaign, we also observed increases in HO_2NO_2 and HNO_3 (Fig. 3), which are consistent with upwind NO_x emissions slowing BrO_x chemistry, and continuing to impact the observed BrO at Utqiaġvik. The more pronounced decrease in BrO mole fractions and ODE frequency for air masses directly impacted by fresh NO_x emissions from Utqiaġvik also supports the idea that NO_2 is acting to terminate ozone depletion chemistry driven by BrO_x.

3.4 Alterations to the vertical distribution of BrO

For both the clean air and non-local wind sectors, the distribution of BrO f_{200} is relatively constant with median values of roughly 30% being in the lowest 200 m of the atmosphere (Fig. 6). In contrast, air masses that are influenced by Utqiaġvik have a median f_{200} of 10%, suggesting the impacts of local emissions on BrO observations are predominantly confined to the lowest 200 m, consistent with the

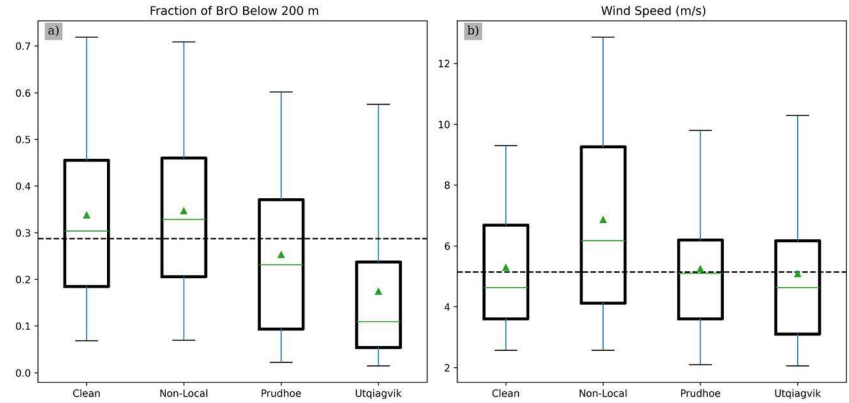

Fig. 6 Box and whisker plots of the fraction of BrO in the lowest 200 m (a), and wind speed (b) binned by air mass categorization. The whiskers extend from the 5th to 95th percentile and the black box bins the 25th to 50th percentile. Means and medians for each bin are indicated with green triangles and lines respectively. All plots show the median for the overall data set with a dashed line.

typically stable boundary layer conditions as well as the short time for vertical mixing or transport. Observations associated with the Prudhoe Bay sector lie between these two cases, with a median f_{200} of 23%. Median BrO mole fractions retrieved for observations impacted by Prudhoe Bay are 85% lower than those in the clean air sector, compared to a 60% decrease in the overall LT-VCD. The vertical distribution of BrO observed at Utqiaġvik depends on many factors including atmospheric stability,[31] the presence of nearby leads which enhance convective mixing in the immediate vicinity,[32,51] and the presence of aerosol particles aloft enabling the propagation of reactive bromine aloft.[9,32,35] Given the location of Utqiaġvik at the northernmost point in Alaska, it is unlikely that there is substantial variability in synoptic scale sea ice conditions. Evaluations of wind speed (Fig. 6) only show a statistically significant difference from the overall dataset in the non-local sector which has a similar BrO f_{200} to the clean air sector. This suggests differences in wind speed are not responsible for the differences observed in the BrO f_{200}. An analysis of aerosol optical thickness retrieved as part of the BrO retrieval (Fig. 5d) also did not show any sector specific dependence, however it should be noted that these retrievals do not provide any information on the chemical composition or mixing state of the aerosol particles which does vary between sectors.[27,28,52]

The depletion of BrO near the surface reflected in a low f_{200} has also been attributed to a repartitioning of BrO_x under low ozone conditions in prior studies. The ozone mole fractions required to alter the partitioning between Br atoms and BrO are generally less than 3 nmol mol^{-1}.[6] However, both of these sectors have higher median observed ozone and only a small number of observations are low enough to be considered depleted (Fig. 5). Thus, re-partitioning of BrO_x driven by low ozone is unlikely to be responsible for the observed changes in BrO vertical distribution in sectors more impacted by NO_x emissions. The impacts of NO_x emissions being confined to the lower part of the observed column is also consistent with observations of enhanced BrCN, a product of the reaction of

reactive bromine with reduced nitrogen compounds,[53] in the polar boundary layer. These findings suggest that NO_x emissions, and potentially concurrent particulate matter emissions, are likely responsible for the altered vertical profile of BrO observed in the Prudhoe Bay and Utqiaġvik categories. This NO_x driven alteration of the BrO profile was also observed during the 2012 Bromine Ozone Mercury EXperiement (BROMEX) during a flight over Prudhoe Bay.[10] This work confirms the behavior observed on this flight day is typical and that these impacts persist 300 km downwind in Utqiaġvik.

4 Conclusions

Five years of springtime BrO observations at Utqiaġvik Alaska show clear impacts of both local and non-local NO_x emissions on the atmospheric bromine chemistry that is a prevalent feature of the springtime Arctic. These impacts include increases in boundary layer ozone due to less active bromine chemistry, as reflected in the decrease in the observed BrO LT-VCD when air masses have interacted with Utqiaġvik or upwind oil and gas extraction facilities. Both findings are consistent with a decreasing chain length and slowed bromine chemistry. These findings also reflect the conversion of BrO_x into other species that cannot be constrained with remote sensing like $BrONO_2$ and $BrNO_2$. The vertical distribution of the observed BrO columns shows that these impacts are predominantly observed in the lowest part of the column, with a greater fraction of BrO being observed aloft during these impacted time periods. While this work focuses on the impacts of oil and gas extraction on the North Slope of Alaska on BrO observations at Utqiaġvik, these activities are prevalent across the Arctic,[54] and are expected to increase.[55]

Given the key role satellite based observations of BrO play in informing our understanding of the basin scale impacts of atmospheric bromine chemistry, it is imperative to understand how these NO_x emissions impact BrO observations, and the degree to which the impacted BrO observations reflect the total amount of reactive bromine species in the boundary layer on a regional scale. These findings suggest BrO observations downwind of these NO_x emissions could be a less effective constraint of active bromine chemistry in modeling studies if these NO_x emissions are not accounted for. While this work focuses on bromine, and other studies have shown the impacts of NO_x emission on downwind chlorine chemistry,[24] relatively little information exists on the interactions with iodine and NO_x emissions. Given the role of iodine in ozone depletion chemistry,[56,57] studies with a focus on iodine are needed to improve our understanding of the coupling between halogen radical chemistry and NO_x cycles. In addition to new measurements, a reexamination of prior halogen measurements in light of these findings may further improve our understanding of the impact of these emissions on naturally occurring photochemical processes across the Arctic and how they may evolve going forward.

Data availability

The CIMS and MAX-DOAS datasets supporting the findings of this study are archived at the National Science Foundation's Arctic Data Center at **https://**

doi.org/10.18739/A2ZC7RT62 (CIMS) and https://doi.org/10.18739/A29882N5H (MAX-DOAS).

Author contributions

Peter Peterson: conceptualization, methodology, formal analysis, writing – original draft preparation; Kerri Pratt: supervision, data curation, writing – review and editing; Paul Shepson: supervision, writing – review and editing; William Simpson: data curation, writing – review and editing.

Conflicts of interest

There are no conflicts to declare.

Acknowledgements

Financial support for collection of the measurement datasets utilized in this work was provided by the National Science Foundation Arctic Natural Sciences program (PLR-1417668, PLR-1417906, ARC-1023118) and the National Aeronautics and Space Administration Cryospheric Sciences Program. The authors gratefully acknowledge the NOAA GMD for their work on the ozone measurements at Utqiaġvik as well as the contributions of Angela Raso (Purdue University, University of Michigan) and Stephen McNamara (University of Michigan) collecting the CIMS data during the PHOXMELT campaign.

References

1 K. A. Pratt, *Trends Chem.*, 2019, **1**, 545–548.
2 W. R. Simpson, R. von Glasow, K. Riedel, P. Anderson, P. Ariya, J. Bottenheim, J. Burrows, L. J. Carpenter, U. Frieß, M. E. Goodsite, D. Heard, M. Hutterli, H.-W. Jacobi, L. Kaleschke, B. Neff, J. Plane, U. Platt, A. Richter, H. Roscoe, R. Sander, P. Shepson, J. Sodeau, A. Steffen, T. Wagner and E. Wolff, *Atmos. Chem. Phys.*, 2007, **7**, 4375–4418.
3 A. Steffen, T. Douglas, M. Amyot, P. Ariya, K. Aspmo, T. Berg, J. Bottenheim, S. Brooks, F. Cobbett, A. Dastoor, A. Dommergue, R. Ebinghaus, C. Ferrari, K. Gardfeldt, M. E. Goodsite, D. Lean, A. J. Poulain, C. Scherz, H. Skov, J. Sommar and C. Temme, *Atmos. Chem. Phys.*, 2008, **8**, 1445–1482.
4 K. A. Pratt, K. D. Custard, P. B. Shepson, T. A. Douglas, D. Pöhler, S. General, J. Zielcke, W. R. Simpson, U. Platt, D. J. Tanner, L. Gregory Huey, M. Carlsen and B. H. Stirm, *Nat. Geosci.*, 2013, **6**, 351–356.
5 K. D. Custard, A. R. W. Raso, P. B. Shepson, R. M. Staebler and K. A. Pratt, *ACS Earth Space Chem.*, 2017, **1**, 142–151.
6 S. Wang, S. M. McNamara, C. W. Moore, D. Obrist, A. Steffen, P. B. Shepson, R. M. Staebler, A. R. W. Raso and K. A. Pratt, *Proc. Natl. Acad. Sci. U. S. A.*, 2019, **116**, 14479–14484.
7 J. P. D. Abbatt, J. L. Thomas, K. Abrahamsson, C. Boxe, A. Granfors, A. E. Jones, M. D. King, A. Saiz-Lopez, P. B. Shepson, J. Sodeau, D. W. Toohey, C. Toubin, R. von Glasow, S. N. Wren and X. Yang, *Atmos. Chem. Phys.*, 2012, **12**, 6237–6271.

8 W. R. Simpson, L. Alvarez-Aviles, T. A. Douglas, M. Sturm and F. Domine, *Geophys. Res. Lett.*, 2005, **32**, L04811.
9 P. K. Peterson, D. Pöhler, H. Sihler, J. Zielcke, S. General, U. Frieß, U. Platt, W. R. Simpson, S. V. Nghiem, P. B. Shepson, B. H. Stirm, S. Dhaniyala, T. Wagner, D. R. Caulton, J. D. Fuentes and K. A. Pratt, *Atmos. Chem. Phys.*, 2017, **17**, 7567–7579.
10 K. D. Custard, C. R. Thompson, K. A. Pratt, P. B. Shepson, J. Liao, L. G. Huey, J. J. Orlando, A. J. Weinheimer, E. Apel, S. R. Hall, F. Flocke, L. Mauldin, R. S. Hornbrook, D. Pöhler, S. General, J. Zielcke, W. R. Simpson, U. Platt, A. Fried, P. Weibring, B. C. Sive, K. Ullmann, C. Cantrell, D. J. Knapp and D. D. Montzka, *Atmos. Chem. Phys.*, 2015, **15**, 10799–10809.
11 G. Deiber, C. George, S. Le Calvé, F. Schweitzer and P. Mirabel, *Atmos. Chem. Phys.*, 2004, **4**, 1291–1299.
12 S. Wang and K. A. Pratt, *J. Geophys. Res.:Atmos.*, 2017, **122**, 11991–12007.
13 R. E. Honrath, Y. Lu, M. C. Peterson, J. E. Dibb, M. A. Arsenault, N. J. Cullen and K. Steffen, *Atmos. Environ.*, 2002, **36**, 2629–2640.
14 A. M. Grannas, A. E. Jones, J. Dibb, M. Ammann, C. Anastasio, H. J. Beine, M. Bergin, J. Bottenheim, C. S. Boxe, G. Carver, G. Chen, J. H. Crawford, F. Dominé, M. M. Frey, M. I. Guzmán, D. E. Heard, D. Helmig, M. R. Hoffmann, R. E. Honrath, L. G. Huey, M. Hutterli, H. W. Jacobi, P. Klán, B. Lefer, J. McConnell, J. Plane, R. Sander, J. Savarino, P. B. Shepson, W. R. Simpson, J. R. Sodeau, R. von Glasow, R. Weller, E. W. Wolff and T. Zhu, *Atmos. Chem. Phys.*, 2007, **7**, 4329–4373.
15 W. N. Meier and J. Stroeve, *Oceanography*, 2022, **35**, 10–19.
16 J. J. Corbett, D. A. Lack, J. J. Winebrake, S. Harder, J. A. Silberman and M. Gold, *Atmos. Chem. Phys.*, 2010, **10**, 9689–9704.
17 K. Bognar, X. Zhao, K. Strong, R. Y.-W. Chang, U. Frieß, P. L. Hayes, A. McClure-Begley, S. Morris, S. Tremblay and A. Vicente-Luis, *J. Geophys. Res.:Atmos.*, 2020, **125**, e2020JD033015.
18 J. W. Halfacre, T. N. Knepp, P. B. Shepson, C. R. Thompson, K. A. Pratt, B. Li, P. K. Peterson, S. J. Walsh, W. R. Simpson, P. A. Matrai, J. W. Bottenheim, S. Netcheva, D. K. Perovich and A. Richter, *Atmos. Chem. Phys.*, 2014, **14**, 4875–4894.
19 P. K. Peterson, W. R. Simpson and S. V. Nghiem, *J. Geophys. Res.:Atmos.*, 2016, **121**, 1381–1396.
20 J. A. Burd, P. K. Peterson, S. V. Nghiem, D. K. Perovich and W. R. Simpson, *J. Geophys. Res.:Atmos.*, 2017, **122**, 8297–8309.
21 W. F. Swanson, K. A. Graham, J. W. Halfacre, C. D. Holmes, P. B. Shepson and W. R. Simpson, *J. Geophys. Res.:Atmos.*, 2020, **125**, e2019JD032139.
22 D. A. Jaffe, R. E. Honrath, J. A. Herring, S.-M. Li and J. D. Kahl, *J. Geophys. Res.:Atmos.*, 1991, **96**, 7395–7405.
23 D. A. Jaffe, R. E. Honrath, D. Furness, T. J. Conway, E. Dlugokencky and L. P. Steele, *J. Atmos. Chem.*, 1995, **20**, 213–227.
24 S. M. McNamara, A. R. W. Raso, S. Wang, S. Thanekar, E. J. Boone, K. R. Kolesar, P. K. Peterson, W. R. Simpson, J. D. Fuentes, P. B. Shepson and K. A. Pratt, *Environ. Sci. Technol.*, 2019, **53**, 8057–8067.
25 J. M. Harris, E. J. Dlugokencky, S. J. Oltmans, P. P. Tans, T. J. Conway, P. C. Novelli, K. W. Thoning and J. D. W. Kahl, *J. Geophys. Res.:Atmos.*, 2000, **105**, 17267–17278.

26 H. A. Bridgman, R. C. Schnell, J. D. Kahl, G. A. Herbert and E. Joranger, *Atmos. Environ.*, 1989, **23**, 2537–2549.
27 K. R. Kolesar, J. Cellini, P. K. Peterson, A. Jefferson, T. Tuch, W. Birmili, A. Wiedensohler and K. A. Pratt, *Atmos. Environ.*, 2017, **152**, 146–155.
28 M. J. Gunsch, R. M. Kirpes, K. R. Kolesar, T. E. Barrett, S. China, R. J. Sheesley, A. Laskin, A. Wiedensohler, T. Tuch and K. A. Pratt, *Atmos. Chem. Phys.*, 2017, **17**, 10879–10892.
29 B. Fasoli, J. C. Lin, D. R. Bowling, L. Mitchell and D. Mendoza, *Geosci. Model Dev.*, 2018, **11**, 2813–2824.
30 G. Hönninger, C. von Friedeburg and U. Platt, *Atmos. Chem. Phys.*, 2004, **4**, 231–254.
31 P. K. Peterson, W. R. Simpson, K. A. Pratt, P. B. Shepson, U. Frieß, J. Zielcke, U. Platt, S. J. Walsh and S. V. Nghiem, *Atmos. Chem. Phys.*, 2015, **15**, 2119–2137.
32 W. R. Simpson, P. K. Peterson, U. Frieß, H. Sihler, J. Lampel, U. Platt, C. Moore, K. Pratt, P. Shepson, J. Halfacre and S. V. Nghiem, *Atmos. Chem. Phys.*, 2017, **17**, 9291–9309.
33 U. Frieß, P. S. Monks, J. J. Remedios, A. Rozanov, R. Sinreich, T. Wagner and U. Platt, *J. Geophys. Res.*, 2006, **111**, D14203.
34 C. D. Rodgers, *Inverse Methods For Atmospheric Sounding: Theory and Practice*, World Scientific, Singapore, 2000.
35 U. Frieß, H. Sihler, R. Sander, D. Pöhler, S. Yilmaz and U. Platt, *J. Geophys. Res.*, 2011, **116**, D00R04.
36 S. Yilmaz, PhD thesis, University of Heidelberg, 2012.
37 W. Simpson, *Atmospheric Measurements via Multiple Axis Differential Optical Absorption Spectroscopy (MAXDOAS), Utqiagvik (Barrow), Alaska 2012-2018*, Arctic Data Center, 2018, DOI: **10.18739/A29882N5H**.
38 J. Liao, H. Sihler, L. G. Huey, J. A. Neuman, D. J. Tanner, U. Friess, U. Platt, F. M. Flocke, J. J. Orlando, P. B. Shepson, H. J. Beine, A. J. Weinheimer, S. J. Sjostedt, J. B. Nowak, D. J. Knapp, R. M. Staebler, W. Zheng, R. Sander, S. R. Hall and K. Ullmann, *J. Geophys. Res.*, 2011, **116**, D00R02.
39 S. McNamara, K. Pratt and P. Shepson, *Photochemical Halogen and Ozone Experiment: Mass Exchange in the Lower Troposphere, Utqiagvik (Barrow), Alaska, 2016*, Arctic Data Center, 2019, DOI: **10.18739/A2ZC7RT62**.
40 A. McClure-Begley, I. Petropavlovskikh and S. Oltmans, *NOAA Global Monitoring Surface Ozone Network. 1973-2014*, National Oceanic and Atmospheric Administration, Earth Systems Research Laboratory Global Monitoring Division, Boulder, CO, 2014, DOI: **10.7289/V57P8WBF**.
41 J. G. Murphy, J. A. Thornton, P. J. Wooldridge, D. A. Day, R. S. Rosen, C. Cantrell, R. E. Shetter, B. Lefer and R. C. Cohen, *Atmos. Chem. Phys.*, 2004, **4**, 377–384.
42 M. Hanke, B. Umann, J. Uecker, F. Arnold and H. Bunz, *Atmos. Chem. Phys.*, 2003, **3**, 417–436.
43 P. Shepson and F. Domine, *Chemistry In The Cryosphere (In 2 Parts)*, World Scientific, 2021.
44 S. J. Oltmans, B. J. Johnson and J. M. Harris, *J. Geophys. Res.*, 2012, **117**, D00R18.
45 K. B. Moiseenko, A. V. Vasileva, A. I. Skorokhod, I. B. Belikov, A. Y. Repin and Y. A. Shtabkin, *Earth Space Sci.*, 2021, **8**, e2021EA001762.

46 A. Dekhtyareva, M. Hermanson, A. Nikulina, O. Hermansen, T. Svendby, K. Holmén and R. G. Graversen, *Atmos. Chem. Phys.*, 2022, **22**, 11631–11656.
47 W. R. Simpson, S. S. Brown, A. Saiz-Lopez, J. A. Thornton and R. von Glasow, *Chem. Rev.*, 2015, **115**, 4035–4062.
48 W. R. Simpson, D. Carlson, G. Hönninger, T. A. Douglas, M. Sturm, D. Perovich and U. Platt, *Atmos. Chem. Phys.*, 2007, **7**, 621–627.
49 P. K. Peterson, D. Pöhler, J. Zielcke, S. General, U. Frieß, U. Platt, W. R. Simpson, S. V. Nghiem, P. B. Shepson, B. H. Stirm and K. A. Pratt, *ACS Earth Space Chem.*, 2018, **2**, 1075–1086.
50 C. R. Thompson, P. B. Shepson, J. Liao, L. G. Huey, C. Cantrell, F. Flocke and J. Orlando, *Atmos. Chem. Phys.*, 2017, **17**, 3401–3421.
51 C. W. Moore, D. Obrist, A. Steffen, R. M. Staebler, T. A. Douglas, A. Richter and S. V. Nghiem, *Nature*, 2014, **506**, 81–84.
52 R. M. Kirpes, A. L. Bondy, D. Bonanno, R. C. Moffet, B. Wang, A. Laskin, A. P. Ault and K. A. Pratt, *Atmos. Chem. Phys.*, 2018, **18**, 3937–3949.
53 J. M. Roberts, S. Wang, P. R. Veres, J. A. Neuman, M. A. Robinson, I. Bourgeois, J. Peischl, T. B. Ryerson, C. R. Thompson, H. M. Allen, J. D. Crounse, P. O. Wennberg, S. R. Hall, K. Ullmann, S. Meinardi, I. J. Simpson and D. Blake, *Atmos. Chem. Phys.*, 2024, **24**, 3421–3443.
54 J. Schmale, S. R. Arnold, K. S. Law, T. Thorp, S. Anenberg, W. R. Simpson, J. Mao and K. A. Pratt, *Earth's Future*, 2018, **6**, 1385–1412.
55 D. L. Gautier, K. J. Bird, R. R. Charpentier, A. Grantz, D. W. Houseknecht, T. R. Klett, T. E. Moore, J. K. Pitman, C. J. Schenk, J. H. Schuenemeyer, K. Sørensen, M. E. Tennyson, Z. C. Valin and C. J. Wandrey, *Science*, 2009, **324**, 1175–1179.
56 A. R. W. Raso, K. D. Custard, N. W. May, D. Tanner, M. K. Newburn, L. Walker, R. J. Moore, L. G. Huey, L. Alexander, P. B. Shepson and K. A. Pratt, *Proc. Natl. Acad. Sci. U. S. A.*, 2017, **114**, 10053–10058.
57 N. Benavent, A. S. Mahajan, Q. Li, C. A. Cuevas, J. Schmale, H. Angot, T. Jokinen, L. L. J. Quéléver, A.-M. Blechschmidt, B. Zilker, A. Richter, J. A. Serna, D. Garcia-Nieto, R. P. Fernandez, H. Skov, A. Dumitrascu, P. Simões Pereira, K. Abrahamsson, S. Bucci, M. Duetsch, A. Stohl, I. Beck, T. Laurila, B. Blomquist, D. Howard, S. D. Archer, L. Bariteau, D. Helmig, J. Hueber, H.-W. Jacobi, K. Posman, L. Dada, K. R. Daellenbach and A. Saiz-Lopez, *Nat. Geosci.*, 2022, **15**, 770–773.

